



**ENHANCING SUPERCONDUCTING PROPERTIES AND GRAIN
CONNECTIVITY OF MAGNESIUM DIBORIDE VIA DOPANT ADDITIONS**

By

NURHIDAYAH BINTI MOHD HAPIPI

**Thesis Submitted to the School of Graduate Studies, Universiti Putra Malaysia, in
Fulfilment of the Requirements for the Degree of Doctor of Philosophy**

December 2022

FS 2022 65

All material contained within the thesis, including without limitation text, logos, icons, photographs and all other artwork, is copyright material of Universiti Putra Malaysia unless otherwise stated. Use may be made of any material contained within the thesis for non-commercial purposes from the copyright holder. Commercial use of material may only be made with the express, prior, written permission of Universiti Putra Malaysia.

Copyright © Universiti Putra Malaysia



DEDICATION

This work is dedicated to my beloved father and mother

**MOHD HAPIPI BIN HANAFI
ASPALILA BINTI JUSOH**

and to my sibling

**NORHIWANI BINTI MOHD HAPIPI
MOHD IQRAM BIN MOHD HAPIPI
NURHIDAYATI BINTI MOHD HAPIPI**

Thank you for everything!

Abstract of thesis presented to the Senate of Universiti Putra Malaysia in fulfilment of the requirement for the degree of Doctor of Philosophy

ENHANCING SUPERCONDUCTING PROPERTIES AND GRAIN CONNECTIVITY OF MAGNESIUM DIBORIDE VIA DOPANT ADDITIONS

By

NURHIDAYAH BINTI MOHD HAPIPI

December 2022

Chair : Chen Soo Kien, PhD
Faculty : Science

In this work, both *ex-situ* and *in-situ* methods were used to synthesise MgB₂ samples. Pure *ex-situ* MgB₂ sample (Series 1) was sintered at various temperatures (600-900 °C) and times (1-7 h). Several dopants such as excess Mg (Series 2), (1.5 Mg + 2 B) (Series 3), nano-Si (Series 4), nano-Si + LaB₆ (Series 5), and Dy₂O₃ + La₂O₃ (Series 6) were added into MgB₂. For series 1, increasing the sintering temperature to 900 °C increased the J_c value (0 T, 20 K) to 4.2×10^3 A/cm², suggesting an enhancement in sample grain coupling. A prolonged sintering time of 3 h increased the J_c value to 3.2×10^3 A/cm² before decreasing to 0.5×10^3 A/cm² when the sintering time was prolonged to 7 h. Meanwhile, the addition of excess Mg into *ex-situ* MgB₂ (Series 2) successfully inhibits MgB₂ decomposition where no MgB₄ peaks were observed in the Mg-added sample, in contrast to pure *ex-situ* MgB₂ which exhibited MgB₄ peaks at higher sintering temperatures. When the sintering temperature increased, the addition of excess Mg reduced the average grain sizes and further strengthened the grain coupling of the samples, which subsequently increased the J_c value to 10^4 A/cm², which is more than 20 times. In Series 3, the addition of 0 to 50 wt.% of (1.5 Mg + 2 B) increased the J_c (0 T, 20 K) value from 3.0×10^3 A/cm² to 1.3×10^4 A/cm², respectively. The highest J_c (0 T, 20 K) value obtained for Series 3 was 2.1×10^4 A/cm² for the sample sintered at 1000 °C. XRD pattern for nano-Si added into *in-situ* MgB₂ samples (Series 4) shows the formation of Mg₂Si where excess Mg₂Si can obstruct the current pathway of the samples and lower the value of J_c . The addition of nano-Si from 0 to 10 wt.% decreased the value of J_c (0 T, 20 K) from 2.4×10^5 A/cm² to 1.7×10^5 A/cm², respectively. However, the J_c value at high field increased to 2.8×10^3 A/cm² with the addition of 5 wt.% of nano-Si. The co-addition of 0.03 mol LaB₆ and x wt.% nano-Si (Series 5) inhibited the grain growth of the samples as no significant changes in average grain size were observed. The addition of LaB₆ decreased J_c (0 T, 20 K) to 2.12×10^5 A/cm², and it further decreased to 1.7×10^5 A/cm² with co-addition of LaB₆ and 10 wt.% of nano-Si. Co-addition of Dy₂O₃ and La₂O₃ into MgB₂ (Series 6) enhanced the flux pinning of the samples and the J_c value, where the highest J_c (0 T, 20 K) value obtained was 4.3×10^5 A/cm² for 1.00 wt.% co-added samples.

Abstrak tesis yang dikemukakan kepada Senat Universiti Putra Malaysia sebagai memenuhi keperluan untuk ijazah Doktor Falsafah

MENINGKATKAN SIFAT MENSUPERKONDUKSI DAN SAMBUNGAN BUTIRAN MAGNESIUM DIBORIDE MELALUI TAMBAHAN BAHAN DOP

Oleh

NURHIDAYAH BINTI MOHD HAPIPI

Disember 2022

Pengerusi : Chen Soo Kien, PhD
Fakulti : Sains

Di dalam kerja ini, kedua-dua kaedah *ex-situ* dan *in-situ* telah digunakan untuk mensintesis sampel MgB₂. Sampel MgB₂ *ex-situ* tulen (Siri 1) telah disinter pada pelbagai suhu (600-900 °C) dan masa (1-7 jam). Beberapa dopan seperti Mg berlebihan (Siri 2), (1.5 Mg + 2 B) (Siri 3), nano-Si (Siri 4), nano-Si + LaB₆ (Siri 5), dan Dy₂O₃ + La₂O₃ (Siri 6) telah ditambah ke dalam MgB₂. Untuk siri 1, peningkatan suhu pensinteran kepada 900 °C telah meningkatkan nilai J_c (0 T, 20 K) kepada 4.2×10^3 A/cm², mencadangkan peningkatan dalam gandingan butiran sampel. Masa pensinteran yang berpanjangan selama 3 jam telah meningkatkan nilai J_c kepada 3.2×10^3 A/cm² sebelum berkurangan kepada 0.5×10^3 A/cm² apabila masa pensinteran dipanjangkan kepada 7 jam. Sementara itu, penambahan Mg berlebihan ke dalam MgB₂ *ex-situ* (Siri 2) berjaya menghalang penguraian MgB₂ di mana tiada puncak MgB₄ diperhatikan dalam sampel tambah Mg, berbeza dengan MgB₂ *ex-situ* tulen yang mempamerkan puncak MgB₄ pada suhu pensinteran yang lebih tinggi. Apabila suhu pensinteran meningkat, penambahan Mg berlebihan telah mengurangkan saiz butiran purata dan mengukuhkan lagi gandingan butiran sampel, yang seterusnya meningkatkan nilai J_c kepada 10^4 A/cm² iaitu lebih daripada 20 kali ganda. Dalam Siri 3, penambahan 0 hingga 50 wt.% daripada (1.5 Mg + 2 B) meningkatkan nilai J_c (0 T, 20 K) daripada 3.0×10^3 A/cm² kepada 1.3×10^4 A/cm², masing-masing. Nilai J_c (0 T, 20 K) tertinggi yang diperolehi untuk Siri 3 ialah 2.1×10^4 A/cm² untuk sampel yang disinter pada 1000 °C. Corak XRD untuk nano-Si ditambah ke dalam sampel MgB₂ *in-situ* (Siri 4) menunjukkan pembentukan Mg₂Si di mana Mg₂Si berlebihan boleh menghalang laluan arus sampel dan menurunkan nilai J_c . Penambahan nano-Si daripada 0 hingga 10 wt.% telah menurunkan nilai J_c (0 T, 20 K) daripada 2.4×10^5 A/cm² kepada 1.7×10^5 A/cm², masing-masing. Walau bagaimanapun, nilai J_c pada medan tinggi telah meningkat kepada 2.8×10^3 A/cm² dengan penambahan 5 wt.% nano-Si. Penambahan bersama 0.03 mol LaB₆ dan x wt.% nano-Si (Siri 5) menghalang pertumbuhan butiran sampel kerana tiada perubahan ketara dalam saiz purata butiran dapat diperhatikan. Penambahan LaB₆ mengurangkan J_c (0 T, 20 K) kepada 2.12×10^5 A/cm², dan ia terus menurun kepada 1.7×10^5 A/cm² dengan penambahan bersama LaB₆ dan 10 wt.% nano-Si. Penambahan bersama Dy₂O₃ dan

La₂O₃ ke dalam MgB₂ (Siri 6) telah meningkatkan penyematan fluks sampel dan nilai J_c , di mana nilai J_c (0 T, 20 K) tertinggi yang diperolehi ialah 4.3×10^5 A/cm² untuk 1.00 wt.% sampel ditambah bersama.



ACKNOWLEDGEMENT

Praise and thanks to Allah for blessing me much more than I deserve.

First, I would like to thank my amazing family, especially my parents for always loving and supporting me. Without their love and support none of this would have been possible. They have always been there for me, and I am thankful for everything. I would like to express my deepest thanks to my supervisor, Assoc. Prof. Dr Chen Soo Kien for the help and kind supervision throughout my research. I am truly fortunate and grateful to have you as my supervisor. A special thank you to my co-supervisor Assoc. Prof. Dr Mohd Mustafa Awang Kechik and Assoc. Prof. Dr Tan Kar Ban. Not forgetting, this special thanks also goes to Assoc. Prof. Dr Lim Kean Pah and Prof. Dr Abdul Halim Shaari for all the help and knowledge given throughout my study.

I would also like to express my thanks to all the staff at the Faculty of Science, UPM, especially, Pn. Nik Afida and Pn. Wan Nor Najwa, for their help and contributions. Finally, thank you to all my wonderful superconductor family members and my fellow friends for always making me laugh a little louder, smile a little wider, and live a little better. Thank you to everyone who takes part in my PhD journey. Special appreciation to the Graduate Research Fellowship (GRF) under School Graduate of Studies and the Special Graduate Research Allowance Scheme for financial support throughout my studies.

This thesis was submitted to the Senate of Universiti Putra Malaysia and has been accepted as fulfilment of the requirement for the degree of Doctor of Philosophy. The members of the Supervisory Committee were as follows:

Chen Soo Kien, PhD

Associate Professor
Faculty of Science
Universiti Putra Malaysia
(Chairman)

Mohd Mustafa Bin Awang Kechik, PhD

Associate Professor
Faculty of Science
Universiti Putra Malaysia
(Member)

Tan Kar Ban, PhD

Associate Professor, ChM.
Faculty of Science
Universiti Putra Malaysia
(Member)

ZALILAH MOHD SHARIFF, PhD

Professor and Dean
School of Graduate Studies
Universiti Putra Malaysia

Date: 11 May 2023

Declaration by the Graduate Student

I hereby confirm that:

- this thesis is my original work;
- quotations, illustrations and citations have been duly referenced;
- this thesis has not been submitted previously or concurrently for any other degree at any institutions;
- intellectual property from the thesis and the copyright of the thesis are fully-owned by Universiti Putra Malaysia, as stipulated in the Universiti Putra Malaysia (Research) Rules 2012;
- written permission must be obtained from the supervisor and the office of the Deputy Vice-Chancellor (Research and innovation) before the thesis is published in any written, printed or electronic form (including books, journals, modules, proceedings, popular writings, seminar papers, manuscripts, posters, reports, lecture notes, learning modules or any other materials) as stated in the Universiti Putra Malaysia (Research) Rules 2012;
- there is no plagiarism or data falsification/fabrication in the thesis, and scholarly integrity is upheld in accordance with the Universiti Putra Malaysia (Graduate Studies) Rules 2003 (Revision 2015-2016) and the Universiti Putra Malaysia (Research) Rules 2012. The thesis has undergone plagiarism detection software

Signature: _____ Date: _____

Name and Matric No.: Nurhidayah Binti Mohd Hapipi

Declaration by Members of the Supervisory Committee

This is to confirm that:

- the research and the writing of this thesis were done under our supervision;
- supervisory responsibilities as stated in the Universiti Putra Malaysia (Graduate Studies) Rules 2003 (Revision 2015-2016) are adhered to.

Signature: _____

Name of Chairman of

Supervisory Committee: _____

Assoc. Prof. Dr Chen Soo Kien

Signature: _____

Name of Member of

Supervisory Committee: _____

Assoc. Prof. Dr Mohd Mustafa Bin Awang Kechik

Signature: _____

Name of Member of

Supervisory Committee: _____

Assoc. Prof. ChM. Dr Tan Kar Ban

TABLE OF CONTENTS

	Page
ABSTRACT	i
ABSTRAK	ii
ACKNOWLEDGEMENT	iv
APPROVAL	v
DECLARATION	vii
LIST OF TABLES	xii
LIST OF FIGURES	xvi
LIST OF ABBREVIATIONS	xxiii
CHAPTER	
1 INTRODUCTION	1
1.1 Background Study	1
1.2 Application of Superconductor	2
1.2.1 Superconducting Wire	2
1.2.2 High-Temperature Superconductor (HTS) Cable	3
1.2.3 Maglev Train	3
1.3 Problem Statement and Research Objective	4
1.4 Thesis Overview	6
2 LITERATURE REVIEW	7
2.1 Method of Synthesizing MgB ₂ Bulk	7
2.1.1 <i>Ex-Situ</i> Method	7
2.1.2 <i>In-Situ</i> Method	8
2.2 Heat Treatment and Phase Formation of MgB ₂	9
2.3 <i>Ex-Situ</i> MgB ₂	9
2.3.1 Crystal Structure and Phase Formation	9
2.3.2 Crystal Microstructure	10
2.3.3 Connectivity, Density, and Porosity	12
2.3.4 Critical Current Density, J_c	13
2.3.5 Superconducting Transition Temperature, T_c	14
2.4 <i>In-Situ</i> MgB ₂	14
2.4.1 Crystal Structure and Phase Formation	14
2.4.2 Crystal Microstructure	15
2.4.3 Connectivity, Density, and Porosity	17
2.4.4 Critical Current Density, J_c	18
2.4.5 Superconducting Transition Temperature, T_c	18
2.5 Addition of Dopants into MgB ₂	19
2.5.1 Addition of Excess Mg	19
2.5.2 Addition of Dy ₂ O ₃ and La ₂ O ₃	20
2.5.3 Addition of SiC and Si	21
3 BASIC PROPERTIES AND THEORY	27
3.1 Introduction to Superconductivity	27
3.1.1 Brief History of Superconductivity	27
3.1.2 Properties of Superconductor	29

3.1.3	Zero Electrical Resistance	29
3.1.4	Ideal Diamagnetism (Meissner Effect)	29
3.1.5	Classification of Superconductor	30
3.1.5.1	Type-I Superconductor	31
3.1.5.2	Type-II Superconductor	32
3.1.6	Critical Current Density, J_c	33
3.1.7	Mixed States and Flux Pinning in the Superconductor	34
3.1.8	Formation of Cooper pairs and BCS Theory	35
3.2	Introduction to MgB ₂ Superconductor	36
3.2.1	History and Background	36
3.2.2	Advantages	38
3.2.3	Crystal Structure	38
3.2.4	Electronic Structure (Two-Gap Superconductor)	39
3.2.5	Applications	40
4	MATERIALS AND METHOD	42
4.1	Introduction	42
4.2	Overall Workflow of the Study	43
4.3	Synthesis of MgB ₂ Powder	45
4.3.1	<i>Ex-situ</i> Method	45
4.3.1.1	Pure MgB ₂ Sample	45
4.3.1.2	Addition of Excess Mg	46
4.3.1.3	Addition of (1.5 mol Mg + 2.0 mol B)	47
4.3.2	<i>In-situ</i> Method (UPM, Malaysia)	48
4.3.2.1	Pure MgB ₂ Sample	48
4.3.2.2	Addition of LaB ₆	49
4.3.2.3	Addition of Nano-Si	49
4.3.2.4	Co-addition of LaB ₆ and Nano-Si	49
4.3.3	<i>In-situ</i> Method (SIT, Japan)	50
4.3.3.1	Pure MgB ₂ Sample	50
4.3.3.2	Co-addition of Dy ₂ O ₃ and La ₂ O ₃	51
4.4	Sample Characterisations	51
4.4.1	X-Ray Diffraction (XRD)	52
4.4.1.1	Crystallite Size	52
4.4.2	Field Emission Scanning Electron Microscopy (FESEM)	53
4.4.3	Superconducting Quantum Interference Device (SQUID) Magnetometer	54
5	RESULTS AND DISCUSSION	55
5.1	Introduction	55
5.2	<i>Ex-situ</i> Method	55
5.2.1	Pure MgB ₂ (Series 1)	55
5.2.1.1	X-ray Diffraction Analysis	55
5.2.1.2	Microstructure Analysis	60
5.2.1.3	Critical Current Density and Flux Pinning Force	63
5.2.1.4	Critical Temperature	66
5.2.2	Addition of Excess Mg (Series 2)	67
5.2.2.1	X-ray Diffraction Analysis	67

5.2.2.2	Microstructure Analysis	71
5.2.2.3	Critical Current Density and Flux Pinning Force	74
5.2.2.4	Critical Temperature	77
5.2.3	Addition of (1.5 mol Mg + 2.0 mol B) (Series 3)	79
5.2.3.1	X-ray Diffraction Analysis	79
5.2.3.2	Microstructure Analysis	83
5.2.3.3	Critical Current Density and Flux Pinning Force	87
5.2.3.4	Critical Temperature	90
5.3	<i>In-situ</i> Method	92
5.3.1	Addition of Nano-Si (Series 4)	92
5.3.1.1	X-ray Diffraction Analysis	92
5.3.1.2	Microstructure Analysis	94
5.3.1.3	Critical Current Density and Flux Pinning Force	96
5.3.1.4	Critical Temperature	98
5.3.2	Co-addition of LaB ₆ and Nano-Si (Series 5)	99
5.3.2.1	X-ray Diffraction Analysis	99
5.3.2.2	Microstructure Analysis	101
5.3.2.3	Critical Current Density and Flux Pinning Force	103
5.3.2.4	Critical Temperature	106
5.3.3	Co-addition of Dy ₂ O ₃ and La ₂ O ₂ S ₃ (Series 6)	107
5.3.3.1	X-ray Diffraction Analysis	107
5.3.3.2	Microstructure Analysis	109
5.3.3.3	Critical Current Density and Flux Pinning Force	113
5.3.3.4	Critical Temperature	115
5.4	Summary	116
6	CONCLUSION	119
6.1	Conclusion	119
6.2	Recommendation and Future Work	120
	BIBLIOGRAPHY	121
	APPENDICES	133
	BIODATA OF STUDENT	141
	LIST OF PUBLICATIONS	142

LIST OF TABLES

Table	Page
2.1 The advantages and disadvantages of the <i>ex-situ</i> method	8
2.2 The advantages and disadvantages of the <i>in-situ</i> method	9
2.3 The compilation of dopant addition in MgB ₂ samples	23
3.1 The critical temperature, T_c for selected type-I and type-II superconducting materials	31
3.2 List of diborides with their respective critical temperature	37
4.1 The mass of chemical materials used to prepare 1 g of mixed powders of <i>ex-situ</i> MgB ₂ and excess Mg	47
4.2 List of all <i>ex-situ</i> MgB ₂ samples added with 0.05 mol Mg sintered at different sintering conditions	47
4.3 The mass of chemical materials used to prepare 1 g of mixed powders of 1.5 mol Mg and 2.0 mol B	48
4.4 List of all <i>ex-situ</i> MgB ₂ samples added with different weight percentages of (1.5 Mg + 2.0 B) sintered at different temperatures for 1 h	48
4.5 The mass of chemical materials used to prepare 1 g of mixed powders of 1 mol Mg and 2 mol B	49
5.1 Intensity fraction of the phases formed of unsintered <i>ex-situ</i> MgB ₂ powder and <i>ex-situ</i> MgB ₂ samples sintered at different temperatures for 1 h	58
5.2 Intensity fraction of the phases formed of <i>ex-situ</i> MgB ₂ samples sintered at 700 °C for different sintering time	58
5.3 Lattice parameter, unit cell volume, and crystallite size of unsintered <i>ex-situ</i> MgB ₂ powder and <i>ex-situ</i> MgB ₂ samples sintered at different temperatures for 1 h	59
5.4 Lattice parameter, unit cell volume and crystallite size of <i>ex-situ</i> MgB ₂ samples sintered at 700 °C for different sintering time	60
5.5 Average grain size for <i>ex-situ</i> MgB ₂ samples sintered at different sintering conditions	63
5.6 Critical current density, J_c , and irreversibility field, H_{irr} at 20 K for <i>ex-situ</i> MgB ₂ samples sintered at different sintering conditions	65

5.7	Onset of critical temperature, $T_{c-onset}$ of <i>ex-situ</i> MgB ₂ sintered at different sintering conditions	67
5.8	Intensity fraction of the phases formed of <i>ex-situ</i> MgB ₂ samples added with 0.5 mol Mg sintered at different temperatures for 1 h	69
5.9	Intensity fraction of the phases formed of <i>ex-situ</i> MgB ₂ samples added with 0.5 mol Mg sintered at 700 °C for different sintering time	69
5.10	Lattice parameter, unit cell volume, and crystallite size of <i>ex-situ</i> MgB ₂ samples added with 0.5 mol Mg sintered at different temperatures for 1 h	70
5.11	Lattice parameter, unit cell volume and crystallite size of <i>ex-situ</i> MgB ₂ samples added with 0.5 mol Mg sintered at 700 °C for different sintering time	70
5.12	Average grain size for <i>ex-situ</i> MgB ₂ added with 0.5 mol Mg samples sintered at different sintering conditions	74
5.13	Critical current density, J_c , and irreversibility field, H_{irr} at 20 K for <i>ex-situ</i> MgB ₂ samples added with 0.5 mol Mg sintered at different sintering conditions	76
5.14	Onset of critical temperature, $T_{c-onset}$ of <i>ex-situ</i> MgB ₂ samples added with 0.5 mol Mg sintered at different sintering conditions	78
5.15	Intensity fraction of <i>ex-situ</i> MgB ₂ added with different weight percentages of (1.5 Mg + 2.0 B) sintered at 700 °C for 1 h	80
5.16	Intensity fraction of <i>ex-situ</i> MgB ₂ added with 30 wt.% of (1.5 Mg + 2.0 B) sintered at different temperatures for 1 h	81
5.17	Lattice parameter, unit cell volume, and crystallite size of <i>ex-situ</i> MgB ₂ samples added with different weight percentages of (1.5 Mg + 2.0 B) sintered at 700 °C for 1 h	82
5.18	Lattice parameter, unit cell volume, and crystallite size of <i>ex-situ</i> MgB ₂ samples added with 30 wt.% of (1.5 Mg + 2.0 B) sintered at different temperatures for 1 h	82
5.19	Average grain size for <i>ex-situ</i> MgB ₂ added with different weight percentages of (1.5 Mg + 2.0 B) sintered at 700 °C for 1 h	85
5.20	Average grain size for <i>ex-situ</i> MgB ₂ added with 30 wt. % (1.5 Mg + 2.0 B) sintered at different temperatures for 1 h	86

5.21	Critical current density, J_c , and irreversibility field, H_{irr} at 20 K for <i>ex-situ</i> MgB ₂ added with different weight percentages of (1.5 Mg + 2.0 B) and sintered at 700 °C for 1 h	88
5.22	Critical current density, J_c at 20 K for <i>ex-situ</i> MgB ₂ added with 30 wt.% of (1.5 Mg + 2.0 B) and sintered at different temperatures for 1 h	89
5.23	Onset of critical temperature, $T_{c-onset}$ of <i>ex-situ</i> MgB ₂ added with different weight percentages of (1.5 Mg + 2.0 B) and sintered at 700 °C for 1 h	91
5.24	Onset of critical temperature, $T_{c-onset}$ of <i>ex-situ</i> MgB ₂ added with 30 wt.% of (1.5 Mg + 2.0 B) and sintered at different temperatures for 1 h	92
5.25	Intensity fraction of <i>in-situ</i> MgB ₂ added with different weight percentages of nano-Si	93
5.26	Lattice parameter, unit cell volume, and crystallite size of <i>in-situ</i> MgB ₂ added with different weight percentages of nano-Si	94
5.27	Average grain size of <i>in-situ</i> MgB ₂ added with different weight percentages of nano-Si	96
5.28	Critical current density, J_c , and irreversibility field, H_{irr} at 20 K for <i>in-situ</i> MgB ₂ samples added with different weight percentages of nano Si	97
5.29	Onset of critical temperature, $T_{c-onset}$ at 20 K for <i>in-situ</i> MgB ₂ samples added with different weight percentages of nano Si	99
5.30	Intensity fraction of <i>in-situ</i> MgB ₂ co-added with LaB ₆ and different weight percentages of nano-Si	101
5.31	Lattice parameter, unit cell volume and crystallite size of <i>in-situ</i> MgB ₂ co-added with LaB ₆ and different weight percentages of nano-Si	101
5.32	Average grain size for <i>in-situ</i> MgB ₂ co-added with LaB ₆ and different weight percentages of nano-Si	103
5.33	Critical current density, J_c , and irreversibility field, H_{irr} at 20 K for <i>in-situ</i> MgB ₂ samples co-added with LaB ₆ and different weight percentages of nano Si	104
5.34	Onset of critical temperature, $T_{c-onset}$ at 20 K for <i>in-situ</i> MgB ₂ samples co-added with LaB ₆ and different weight percentages of nano Si	106

5.35	Intensity fraction of <i>in-situ</i> MgB ₂ samples co-added with <i>x</i> wt.% Dy ₂ O ₃ : <i>x</i> wt.% La ₂ O ₃	108
5.36	Lattice parameter, unit cell volume, and crystallite size of <i>in-situ</i> MgB ₂ samples co-added with <i>x</i> wt.% Dy ₂ O ₃ : <i>x</i> wt.% La ₂ O ₃	109
5.37	Average grain size for <i>in-situ</i> MgB ₂ co-added with <i>x</i> wt.% Dy ₂ O ₃ : <i>x</i> wt.% La ₂ O ₃	112
5.38	Critical current density, J_c , and irreversibility field, H_{irr} at 20 K for MgB ₂ samples co-added with <i>x</i> wt.% Dy ₂ O ₃ : <i>x</i> wt.% La ₂ O ₃	114
5.39	Onset of critical temperature, $T_{c-onset}$ at 20 K for MgB ₂ samples co-added with <i>x</i> wt.% Dy ₂ O ₃ : <i>x</i> wt.% La ₂ O ₃	116

LIST OF FIGURES

Figure		Page
1.1	Comparison of the cross-sectional area for bismuth-based superconductor wire and copper wire carrying the same current magnitude	2
1.2	The illustration of the superconductor Maglev levitation and propulsion system	3
2.1	Backscattered SEM images of samples sintered at (a) 900 °C, (b) 1000 °C, (c) 1100 °C, and (d) 1200 °C at 250× magnification. Four different contrast levels, MgB ₂ (light gray), MgB ₄ (dark grey), MgO (white), and porosity (black) can be observed (Matthews et al., 2020)	11
2.2	SEM images of <i>ex-situ</i> MgB ₂ bulks (a) before and after being sintered at (b) 900 °C (24 h), and (c) 900 °C (240 h). Area A in (a) indicates 'egg' of necks. Areas B and C in (b) indicate a neck and an open pore, respectively (Tanaka et al., 2012)	11
2.3	SEM images <i>ex-situ</i> MgB ₂ sintered at (a) 1000 °C (30 min), and (b) 1050 °C (10 min). The arrows indicate the secondary phase particles (Shim et al., 2005)	12
2.4	SEM images of MgB ₂ bulks sintered at (a) 650 °C (b) 700 °C (c) 750 °C, and (d) at 800 °C (Yan et al., 2004)	16
2.5	SEM images of MgB ₂ superconductor sintered at 775 °C (left) and 805 °C (right) in the argon atmosphere (Kobayashi et al., 2015)	16
2.6	SEM-BSE for (a) low magnification image and (b) high magnification image of MgB ₂ sample sintered at 900 °C for 48 h (Shimada et al., 2016)	17
2.7	SEM images of MgB ₂ powder after 5 h of oxidation at 900 °C indicate long thin MgO whiskers on the grain surface (Yang et al., 2003)	17
2.8	SEM images of (a) pure MgB ₂ (b) MgB ₂ + 10% Mg samples (Wu, 2014)	20
2.9	SEM images for (a) pure, (b) 5 wt.% La ₂ O ₃ , (c) 10 wt.% acetone, and (d) 5 wt.% La ₂ O ₃ + 10 wt.% acetone codoped samples (Gao et al., 2010)	21
3.1	Timeline of discoveries of superconducting materials. Colours symbols represent different classes of materials (Ray, 2015)	28

3.2	The relation between resistances with the temperature at the superconducting state (Adapted from Warren, 2003)	29
3.3	Magnetic levitation phenomenon on superconducting bulk material in liquid nitrogen bath (Meissner effect)	30
3.4	Schematic diagram of magnetic behaviour for type-I superconductor (a) a plot of internal field versus applied magnetic field (b) a plot of magnetisation versus applied magnetic field (Adapted from Rose-Innes and Rhoderick, 1978)	32
3.5	Schematic diagram of magnetic behaviour for type-II superconductor (a) a plot of internal field versus applied magnetic field (b) a plot of magnetisation versus applied magnetic field (Adapted from Rose-Innes and Rhoderick, 1978)	33
3.6	Schematic diagram of the mixed state, showing normal cores (dark regions) and encircling supercurrent vortices in a superconductor (Adapted from Rose-Innes and Rhoderick, 1978)	34
3.7	Schematic diagrams of vortex in type-II superconductor carrying current through the mixed state. The Lorentz force, F_L on magnetic flux is perpendicular both to the axes of the tubes and to the transport current, J (Adapted from Rose-Innes and Rhoderick, 1978)	34
3.8	The formation of the Cooper pair	36
3.9	The hexagonal crystal structure of the MgB_2 compound, consisting of B and Mg atoms (Adapted from Yildirim, 2002)	39
3.10	The sketch of the MgB_2 cable system (Adapted from Bruzek et al., 2017; Bruzek and Marian, 2021)	41
4.1	The flow diagram of <i>ex-situ</i> MgB_2 method	43
4.2	The flow diagram of <i>in-situ</i> MgB_2 method	44
4.3	Commercial MgB_2 powder was ground using mortar and pestle for 1 h	45
4.4	The stainless-steel tube was closed completely using a clamp	46
4.5	Heating and cooling profile for <i>ex-situ</i> MgB_2 heat-treatment process. The heating temperature (labeled as A) varied to 600, 700, 800, 900, and 1000 °C and heat time (labeled as B) varies from 1, 2, 3, 5, and 7 h	46
4.6	The MgB_2 powders were mixed in an argon atmosphere glove box	50
4.7	The pellets were wrapped with titanium foils	50

4.8	Tube furnace connected with argon gas used to heat the samples	51
4.9	Heating and cooling profile for <i>in-situ</i> MgB ₂ heat-treatment process. The heating temperature was fixed to 775 °C and held for 3 h before cooling to room temperature	51
4.10	Scattered X-rays by a crystal lattice (Adapted from Suryanarayana and Norton, 2013)	52
4.11	The schematic diagram of a field emission scanning electron microscope (FESEM)	53
5.1	XRD patterns of unsintered <i>ex-situ</i> MgB ₂ powder	56
5.2	XRD patterns of <i>ex-situ</i> MgB ₂ sintered at different temperatures for 1 h	57
5.3	XRD patterns of <i>ex-situ</i> MgB ₂ sintered at 700 °C for different sintering time	57
5.4	High magnification FESEM images of fractured surfaces of <i>ex-situ</i> MgB ₂ bulk sintered at different temperatures (a) 600 °C (b) 700 °C (c) 900 °C for 1 h. The distribution of grain size is shown on the right-hand side of the images	61
5.5	High magnification FESEM images of fractured surfaces of <i>ex-situ</i> MgB ₂ bulk sintered at 700 °C for (a) 1 h (b) 3 h (c) 7 h. The distribution of grain size is shown on the right-hand side of the images	62
5.6	(a) Field dependence of critical current densities, J_c (20 K) for <i>ex-situ</i> MgB ₂ sintered at different temperatures for 1 h (b) Same plot as (a) with J_c in log scale	63
5.7	(a) Field dependence of critical current densities, J_c (20 K) of <i>ex-situ</i> MgB ₂ sintered at 700 °C for different sintering time (b) Same plot as (a) with J_c in log scale	64
5.8	Comparison of critical current densities, J_c (20 K) between self-field J_c (0 T) and high field J_c (3 T) of <i>ex-situ</i> MgB ₂ sintered at different (a) sintering temperatures and (b) sintering time	64
5.9	Normalized pinning force $F_p/F_{p,max}$ as a function of reduced magnetic field H/H_{irr} at 20 K for <i>ex-situ</i> MgB ₂ sintered at different (a) sintering temperatures and (b) sintering time	65
5.10	(a) Temperature dependence of normalized DC susceptibility (b) plots of $\delta\chi/\delta T$ versus T of <i>ex-situ</i> MgB ₂ sintered at different temperatures for 1 h (left-hand side)	66

5.11	(a) Temperature dependence of normalized DC susceptibility (b) plots of $\delta\chi/\delta T$ versus T of <i>ex-situ</i> MgB ₂ sintered at 700 °C for different sintering times	66
5.12	XRD patterns of <i>ex-situ</i> MgB ₂ samples added with 0.5 mol Mg sintered at different temperatures for 1 h	68
5.13	XRD patterns of <i>ex-situ</i> MgB ₂ samples added with 0.5 mol Mg sintered at 700 °C for different sintering time	68
5.14	High magnification FESEM images of fractured surfaces of <i>ex-situ</i> MgB ₂ bulks added with 0.5 mol Mg sintered at different temperatures (a) 600 °C (b) 700 °C (c) 1000 °C for 1 h, respectively. The distribution of grain size is shown on the right-hand side of the images	72
5.15	High magnification FESEM images of fractured surfaces of <i>ex-situ</i> MgB ₂ bulks added with 0.5 mol Mg sintered at 700 °C, respectively for (a) 1 h (b) 3 h (c) 7 h. The distribution of grain size is shown on the right-hand side of the images	73
5.16	Field dependence of critical current densities, J_c (20 K) of <i>ex-situ</i> MgB ₂ samples added with 0.5 mol Mg sintered at different temperatures for 1 h (b) Same plot as (a) with J_c in log scale	75
5.17	Field dependence of critical current densities, J_c (20 K) of <i>ex-situ</i> MgB ₂ samples added with 0.5 mol Mg sintered at 700 °C for different sintering time (b) Same plot as (a) with J_c in log scale	75
5.18	Comparison of critical current densities, J_c (20 K) between self-field J_c (0 T) and high field J_c (3 T) of <i>ex-situ</i> MgB ₂ samples added with 0.5 mol Mg sintered at different (a) sintering temperatures and (b) sintering time	76
5.19	Normalized pinning force $F_p/F_{p,max}$ as a function of reduced magnetic field H/H_{irr} at 20 K for <i>ex-situ</i> MgB ₂ samples added with 0.5 mol Mg sintered at different (a) sintering temperatures and (b) sintering time	77
5.20	(a) Temperature dependence of normalized DC susceptibility (b) plots of $\delta\chi/\delta T$ versus T of <i>ex-situ</i> MgB ₂ samples added with 0.5 mol Mg sintered at different temperatures for 1 h	78
5.21	(a) Temperature dependence of normalized DC susceptibility (b) plots of $\delta\chi/\delta T$ versus T of <i>ex-situ</i> MgB ₂ samples added with 0.5 mol Mg sintered at 700 °C for different sintering times	78
5.22	XRD patterns of <i>ex-situ</i> MgB ₂ added with different weight percentages of (1.5 Mg + 2.0 B) sintered at 700 °C for 1 h	80

5.23	XRD patterns of <i>ex-situ</i> MgB ₂ added with 30 wt.% of (1.5 Mg + 2.0 B) sintered at different temperatures for 1 h	81
5.24	High magnification FESEM images of fractured surfaces of <i>ex-situ</i> MgB ₂ bulk added with (a) 0 wt.%, (b) 10 wt.%, (c) 30 wt.%, (d) 50 wt.% of (1.5 Mg + 2.0 B), respectively sintered at 700 °C for 1 h. The distribution of grain size is shown on the right-hand side of the images	84
5.25	High magnification FESEM images of fractured surfaces of <i>ex-situ</i> MgB ₂ bulks added with 30 wt.% (1.5 Mg + 2.0 B) sintered at (a) 700 °C, (b) 800 °C, (c) 1000 °C, for 1 h respectively. The distribution of grain size is shown on the right-hand side of the images	85
5.26	Field dependence of critical current densities, J_c (20 K) of <i>ex-situ</i> MgB ₂ added with different weight percentages of (1.5 Mg + 2.0 B) and sintered at 700 °C for 1 h (b) Same plot as (a) with J_c in log scale	87
5.27	Comparison of critical current densities, J_c (20 K) between self-field J_c (0 T) and high field J_c (3 T) of <i>ex-situ</i> MgB ₂ added with (a) different weight percentages of (1.5 Mg + 2.0 B) sintered at 700 °C for 1 h and (b) 30 wt.% (1.5 Mg + 2.0 B) sintered at different temperatures for 1 h	88
5.28	Field dependence of critical current densities, J_c (20 K) of <i>ex-situ</i> MgB ₂ added with 30 wt.% of (1.5 Mg + 2.0 B) and sintered at different temperatures for 1 h (b) Same plot as (a) with J_c in log scale	89
5.29	Normalized pinning force $F_p/F_{p,max}$ as a function of reduced magnetic field H/H_{irr} at 20 K for <i>ex-situ</i> MgB ₂ added with (a) different weight percentages of (1.5 Mg + 2.0 B) sintered at 700 °C for 1 h and (b) 30 wt. % (1.5 Mg + 2.0 B) sintered at different temperatures for 1 h	90
5.30	(a) Temperature dependence of normalized DC susceptibility (b) plots of $\delta\chi/\delta T$ versus T of <i>ex-situ</i> MgB ₂ added with different weight percentages of (1.5 Mg + 2.0 B) and sintered at 700 °C for 1 h	91
5.31	(a) Temperature dependence of normalized DC susceptibility (b) plots of $\delta\chi/\delta T$ versus T of <i>ex-situ</i> MgB ₂ added with 30 wt.% of (1.5 Mg + 2.0 B) and sintered at different temperatures for 1 h	91
5.32	XRD patterns of <i>in-situ</i> MgB ₂ added with different weight percentages of nano-Si	93
5.33	High magnification FESEM images of fractured surfaces of <i>in-situ</i> MgB ₂ added with (a) 0 wt.%, (b) 5 wt.%, (c) 10 wt.% of nano-Si.	95

The distribution of grain size is shown on the right-hand side of the images

5.34	Field dependence of critical current densities, J_c (20 K) of <i>in-situ</i> MgB ₂ samples added with different weight percentages of nano Si (b) Same plot as (a) with J_c in log scale	96
5.35	Comparison of critical current densities, J_c (20 K) between self-field J_c (0 T) and high field J_c (3 T) of <i>in-situ</i> MgB ₂ samples added with different weight percentages of nano-Si	97
5.36	Normalized pinning force $F_p/F_{p,max}$ as a function of reduced magnetic field H/H_{irr} at 20 K for <i>in-situ</i> MgB ₂ added with different weight percentages of nano-Si	98
5.37	(a) Temperature dependence of normalized DC susceptibility (b) plots of $\delta\chi/\delta T$ versus T of <i>in-situ</i> MgB ₂ added with different weight percentages of nano-Si	99
5.38	XRD patterns of <i>in-situ</i> MgB ₂ co-added with LaB ₆ and different weight percentages of nano-Si	100
5.39	High magnification FESEM images of fractured surfaces of (a) pure <i>in-situ</i> MgB ₂ and <i>in-situ</i> MgB ₂ co-added with LaB ₆ and (b) 0 wt.%, (c) 5 wt.% and (d) 10 wt.% of nano-Si. The distribution of grain size is shown on the right-hand side of the images	102
5.40	Field dependence of critical current densities, J_c (20 K) of <i>in-situ</i> MgB ₂ samples co-added with LaB ₆ and different weight percentages of nano-Si (b) Same plot as (a) with J_c in log scale	104
5.41	Comparison of critical current densities, J_c (20 K) between self-field J_c (0 T) and high field J_c (3 T) of <i>in-situ</i> MgB ₂ samples co-added with LaB ₆ and different weight percentages of nano-Si	105
5.42	Normalized pinning force $F_p/F_{p,max}$ as a function of reduced magnetic field H/H_{irr} at 20 K for <i>in-situ</i> MgB ₂ co-added with LaB ₆ and different weight percentages of nano-Si	105
5.43	(a) Temperature dependence of normalized DC susceptibility (b) plots of $\delta\chi/\delta T$ versus T of <i>in-situ</i> MgB ₂ samples co-added with LaB ₆ and different weight percentages of nano-Si	106
5.44	XRD patterns of <i>in-situ</i> MgB ₂ samples co-added with x wt.% Dy ₂ O ₃ : x wt.% La ₂ O ₃	108
5.45	High magnification FESEM images of fractured surfaces of <i>in-situ</i> MgB ₂ bulks added with x wt.% Dy ₂ O ₃ : x wt.% La ₂ O ₃ for (a) $x = 0.0$ wt.% (b) $x = 0.25$ wt.% (c) $x = 0.50$ wt.% (d) $x = 0.75$ wt.% (e) $x =$	110

1.00 wt.%, respectively. The distribution of grain size is shown on the right-hand side of the images

- 5.46 Backscattered FESEM images of fractured surfaces of MgB_2 samples co-added with x wt.% Dy_2O_3 : x wt.% La_2O_3 for (a) $x = 0.0$ wt.% (b) $x = 0.25$ wt.% (c) $x = 0.50$ wt.% (d) $x = 0.75$ wt.%, and (e) $x = 1.00$ wt.%, respectively 112
- 5.47 Field dependence of critical current densities, J_c (20 K) *in-situ* MgB_2 samples co-added with x wt.% Dy_2O_3 : x wt.% La_2O_3 (b) Same plot as (a) with J_c in log scale 113
- 5.48 Comparison of critical current densities, J_c (20 K) between self-field J_c (0 T) and high field J_c (3 T) of MgB_2 samples co-added with x wt.% Dy_2O_3 : x wt.% La_2O_3 114
- 5.49 Normalized pinning force $F_p/F_{p,\text{max}}$ as a function of reduced magnetic field H/H_{irr} at 20 K for MgB_2 samples co-added with x wt.% Dy_2O_3 : x wt.% La_2O_3 115
- 5.50 (a) Temperature dependence of normalized DC susceptibility (b) plots of $\delta\chi/\delta T$ versus T of *in-situ* MgB_2 samples co-added with x wt.% Dy_2O_3 : x wt.% La_2O_3 116

LIST OF ABBREVIATIONS

θ	Angle of diffraction
\AA	Angstrom (Unit of length equal to 10^{-10} m)
H_{ac}	Applied magnetic field
a.u.	Arbitrary unit
ξ	Coherence length
J_c	Critical current density
T_c	Critical temperature
Dy_2O_3	Dysprosium (III) oxide
FESEM	Field emission scanning electron microscopy
FWHM	Full width at half maximum
κ	Ginzburg-Landau constant
HTS	High-temperature superconductor
ICSD	Inorganic Crystal Structure Database
H_{irr}	Irreversibility field
K	Kelvin (Standard unit of temperature)
LaB_6	Lanthanum hexaboride
La_2O_3	Lanthanum (III) oxide
a -, b -, c -axis	Lattice parameter
LTS	Low-temperature superconductor
F_L	Lorentz force
Mg	Magnesium
MgB_2	Magnesium diboride
MgO	Magnesium oxide
Φ_0	Magnetic flux

mol.%	Molar percentage
$T_{c\text{-onset}}$	Onset critical temperature
$T_{c\text{-offset}}$	Offset critical temperature
F_p	Pinning force
Si	Silicone
SQUID	Superconducting Quantum Interference Devices
T	Tesla (Standard unit of magnetic flux density)
TGA	Thermogravimetry Analysis
ΔT_c	Transition temperature width
wt.%	Weight percentage
XRD	X-Ray Diffractometer
λ	X-ray wavelength

CHAPTER 1

INTRODUCTION

1.1 Background Study

Superconductivity is a physical phenomenon that occurs when the electrical resistance of a material is zero and magnetic flux is expelled from the material. Any material that exhibits these properties is known as a superconductor (Rose-Innes and Rhoderick, 1978). Superconductors can be divided into low-temperature superconductors, LTS (niobium-based alloy), and high-temperature superconductors, HTS (copper-oxide-based). If the critical temperature, T_c , of a superconductor is above 30 K, it is classified as HTS. In the meantime, a T_c value below 30 K is referred to as LTS. Many researchers are more interested in studying HTS compared to LTS due to its higher T_c and J_c values.

However, following the discovery of superconductivity in MgB_2 , researchers became interested in studying MgB_2 . This is because MgB_2 has a simple crystal structure and high critical temperature ($T_c \approx 39$ K), making it a most promising candidate for cryogen-free operation to replace conventional NbTi and Nb_3Sn -based technology. Two common methods to prepare MgB_2 bulk samples are *in-situ* (Arvapalli et al., 2019; Gao et al., 2010; Kim et al., 2007; Muralidhar et al., 2017) and *ex-situ* method (Malagoli et al., 2010; Mizutani et al., 2014; Tanaka et al., 2012). *In-situ* is a method of synthesising MgB_2 by simply mixing Mg and B powders at the appropriate ratio of Mg: B = 1: 2. During heat treatment, Mg grains melt and diffuse into B grains through a liquid-solid reaction. Meanwhile, the *ex-situ* method involves heat treatment of the pre-reacted MgB_2 powders. Although commercial MgB_2 powders are readily available as it has been synthesized since the early 1950s, the quality of MgB_2 powder may not be as good as desired (Buzea and Yamashita, 2001).

MgB_2 also possesses a high critical current density, $J_c (> 10^5$ A/cm² at 20 K, 0 T), strong grain coupling due to its large coherence lengths ($\xi_{ab} \sim 6.5$ nm at 0 K), and weak-link-free behaviour at grain boundaries. MgB_2 is a lightweight and inexpensive material that is ideal for commercial and industrial applications (Buzea and Yamashita, 2001; Larbalestier et al., 2001; Xu et al., 2001; Yamamoto et al., 2004; Zhao et al., 2001). However, further improvement of J_c and flux pinning is crucial for the material to be used in high magnetic field applications. Prior studies show the addition of dopants such as Mg (Zeng et al., 2008; Zhang et al., 2015), La (Kimishima et al., 2004; Shekhar et al., 2005), La_2O_3 (Gao et al., 2010), Dy_2O_3 (Chen et al., 2006), Si (Tan et al., 2015; Zhang et al., 2010) and carbon (Ohmichi et al., 2004; Tan et al., 2015; Yeoh et al., 2004) into MgB_2 can act as flux pinning that enhanced the value of J_c , resulting in high-quality MgB_2 samples.

1.2 Applications of Superconductor

Superconductors have brought great success and technological changes, especially in energy storage, transportation, electronics, and medical sector. Some of the applications are discussed as follows:

1.2.1 Superconducting Wire

Superconductor wire is an electrical wire made of superconductor material that exhibits no electrical resistance when cooled below T_c . Figure 1.1 shows that, although bismuth-based superconductor wire has a smaller cross-sectional area than copper wire, it can carry the same current magnitude. It means that superconductor wire can carry approximately 200 times more electric current than copper wire with the same cross-sectional area (Hayashi, 2020).

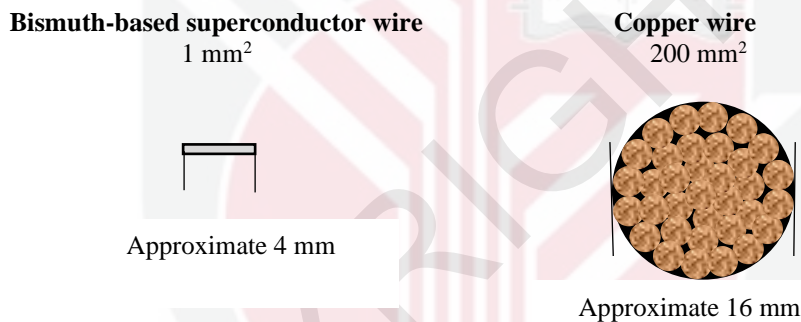


Figure 1.1: Comparison of the cross-sectional area for bismuth-based superconductor wire and copper wire carrying the same current magnitude

Commonly, conventional superconductors such as niobium-titanium (NbTi) and niobium-tin (Nb_3Sn) are used as the superconducting wire. However, these conventional superconductors are made from low-temperature superconductors that require very expensive liquid helium for cooling. Besides, Nb_3Sn is brittle and difficult to fabricate. High-temperature superconductor (HTS) wires were later introduced to the market. HTS wire can operate in liquid nitrogen, which is cheaper than liquid helium. HTS wires are also more tolerant of AC loss and have better thermal stability than low-temperature superconducting (LTS) wires. There are two types of high-temperature superconductor wires: first-generation (1G) wire, bismuth strontium calcium copper oxide, BSCCO, and second-generation (2G) wire, rare-earth barium copper oxide, ReBCO. 1G HTS superconductor wires are widely used on various HTS power devices such as transmission cables, transformers, motors, and generators. The first company to produce long bismuth-based superconductor wire (DI-BSCCO) is Sumitomo Electric Japan. The transition from 1G HTS wire to 2G HTS wires promises that 2G HTS wires will be cheaper than existing 1G wires. This 2G HTS wire provides cost benefits and excellent performance benefits (Hayashi, 2020).

1.2.2 High-Temperature Superconductor (HTS) Cable

High-temperature superconductor (HTS) power cable is made of a group of sheath-coated wires. It can carry two to five times the electrical current more than conventional cables such as XLPE (Cross Link Poly Ethylene) of the same size. Furthermore, HTS cable can operate at high current levels with minimal heat and electricity loss, which aids in energy conservation. HTS cables are also smaller than conventional cables, allowing them to occupy less space. Therefore, it does not require extensive construction work for installation, potentially lowering construction costs. In Japan, the Railway Technical Research Institute (RTRI) has developed a superconducting feeder cable system. This superconducting feeder cable connects the Hino Civil Engineering Testing Station to the regular feeding circuit of the Chuo line (408 m cable), where it needs to be cooled with cryogenic or liquid nitrogen. The test confirmed that currents up to 2200 A or larger could flow from the substation to the test train as the train is accelerated. Most importantly, the shut-off test confirmed that the train could keep running, powered by the regular feeding circuit, even after the superconducting system is shut off (*Superconducting Feeder Cable System*, 2019).

1.2.3 Maglev Train

In the 21st century, few countries such as Japan, South Korea, and China have developed powerful electromagnetic high-speed trains called maglev trains. Maglev is derived from "magnetic" and "levitation". Maglev trains operate on magnetic repulsion principles between a train and a track, where magnetic levitation can be achieved using an electrodynamic suspension system (EDS).

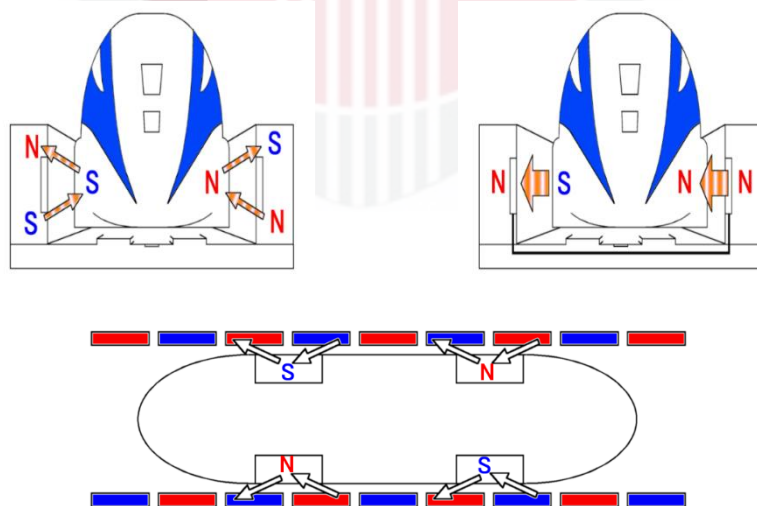


Figure 1.2: The illustration of the superconductor Maglev levitation and propulsion system

Figure 1.2 shows an illustration of the Maglev superconductor levitation and propulsion system. The Maglev train railway consists of two sets of cross-connected metal coils wound into a "figure eight" pattern along both the guideway walls to form electromagnets. These coils are also cross connected underneath the rails to accelerate the cars and guide and stabilise them. Due to the magnetic field induction effect, the magnetic field of the superconducting magnets induces a current into these coils when the train accelerates.

The train's movement starts when it moves forward slowly on the wheels, allowing the magnets beneath the train to interact with the guideway. Once the train reaches 150 kilometres per h, the magnetic force is strong enough to lift the train 4 inches off the ground. The magnetic force will then eliminate friction between the car and the guideway, allowing for faster speeds. This magnetic force also makes the train move forward and continue to be centred within the guideway. If the train is centred with the coils, the electrical potential will be balanced, and no currents will be induced. However, when the train runs on rubber wheels at a lower speed, a magnetic field positioned below the coils' centre will cause an unbalanced electrical potential. When stopped, the train will rest on rubber wheels.

The advantage of the Maglev train is that it can float on the rails, which means there is no rail friction. It allows trains to travel at speeds of hundreds of miles per h. Since the trains rarely touch the track, there is not much noise and vibration compared to regular trains. As a result, the Maglev train produces minor mechanical damage. The Central Japan Railway Company and the Railway Technical Research Institute developed the first Maglev superconductor trains in the 1970s. In April 2015, Japan Railway maglev trains recorded 603 km/h, far faster than Maglev trains operating in Shanghai, China (431 km/h to 500 km/h) and in South Korea (109 km/h). In the latest related development, Chuo Shinkansen maglev line is planned to connect Tokyo and Nagoya by 2027. The Chuo Shinkansen maglev line is expected to cover the 178-mile distance (Tokyo to Nagoya) at 500 km/h, slashing the travel time to just forty minutes. It means that the Chuo Shinkansen maglev line can reduce travel time by around 50% compared to the current Tokaido Shinkansen line.

1.3 Problem Statement and Research Objective

The main problem in the process of synthesising MgB_2 is determining suitable and optimal sintering conditions. This is because the optimal sintering value can reduce the grain size of the sample which increased the flux pinning at the grain boundary and enhanced the grain connectivity of the samples (Kobayashi et al., 2015; Matthews et al., 2020; Tanaka et al., 2012; Yamamoto et al., 2012). Unlike previous studies that varied the sintering conditions at high temperatures (Shim et al., 2005) and for a long time (Tanaka et al., 2012), this study is more focused on shorter sintering time (1-7 h) and lower sintering temperature (600-1000 °C).

Furthermore, another major issue for MgB_2 is that Mg is highly volatile and oxidised, especially at elevated temperatures. Addition of excess Mg is expected to compensate

for the loss of Mg, reduce the formation of the MgO phase, and increase the grain connectivity, which can increase the value of J_c , especially at low temperatures and magnetic fields (Zeng et al., 2008; Zhang et al., 2015). However, prior studies (Arvapalli et al., 2019; Zeng et al., 2008; Zhang et al., 2015) focused on the addition of excess Mg to *in-situ* MgB₂ instead of *ex-situ* MgB₂. Both *in-situ* and *ex-situ* methods have their shortcomings. Although *in-situ* sample has strong grain coupling and easily reaches a high J_c value, it has a low bulk density and low connectivity. Meanwhile, *ex-situ* sample has a higher bulk density, but the grain coupling for *ex-situ* MgB₂ sample is weaker than *in-situ* MgB₂ sample (Li et al., 2012; Yamamoto et al., 2012). Therefore, in this work, both methods are combined to compensate for each other's shortcomings.

It is necessary to further improve the flux pinning and J_c value of MgB₂ sample to make it suitable for high magnetic field applications. This problem can be overcome by introducing dopants such as Si and LaB₆ into MgB₂. The addition of Si into MgB₂ can increase the value of J_c at a higher field (Wang et al., 2003). It has also been claimed that the addition of La₂O₃ resulted in the formation of LaB₆, which acts as an effective pinning center that increased the intragrain J_c (Gao et al., 2010; Shekhar et al., 2005). Hence, this study continues to focus on the co-addition of Si and LaB₆ to improve the flux pinning center and increase the value of J_c at all magnetic fields.

Similar to LaB₆, the formation of DyB₄ (Chen et al., 2006) can act as an effective flux pinning and increase the value of J_c . Although it is important to increase the value of J_c , the addition of dopants should not affect the value of T_c . Studies have shown that the addition of Dy₂O₃ (Chen et al., 2006) or La₂O₃ (Zhao-Shun et al., 2010) did not result in a drastic reduction of T_c , most likely due to the insignificant substitution of the lattice structure of MgB₂. Therefore, the co-addition of Dy₂O₃ and La₂O₃ into MgB₂ is expected to form LaB₆ and DyB₄ which can act as flux pinning centers and further improve the J_c value.

Hence, the objectives of this work are:

- i. To enhance grain coupling of *ex-situ* MgB₂ via optimisation of sintering temperature and time.
- ii. To elucidate the influence of materials addition such as excess Mg and (1.5 mol Mg + 2.0 mol B) on structural and superconducting properties of the *ex-situ* MgB₂.
- iii. To investigate the effects of LaB₆, nano Si and co-addition of LaB₆ and nano-Si on structural and superconducting properties of *in-situ* MgB₂.
- iv. To investigate the effects of co-addition of Dy₂O₃ and La₂O₃ on structural and superconducting properties of *in-situ* MgB₂.

1.4 Thesis Overview

This thesis consists of six chapters. Chapter 1 introduces a brief history of superconductors and their applications. The problem statement and the objectives of this work are also discussed in Chapter 1. Chapter 2 reviews the previous works of MgB₂ superconductors focusing on the preparation methods, heat treatment conditions, and dopant additions used by previous researchers. The theory and fundamentals of superconductivity, especially MgB₂, will be explained in Chapter 3. Chapter 4 focuses on the materials and methods used for this work. Sample characterisation, such as XRD, FESEM, and SQUID measurement, is also discussed in detail. Chapter 5 discusses all the analysed results obtained from all the sample characterisations. Finally, in Chapter 6, the outcomes of this research will be summarised, followed by recommendations for future research.

BIBLIOGRAPHY

- Akimitsu, J., Akutagawa, S., Kawashima, K., and Muranaka, T. (2005). Superconductivity in MgB₂ and its related materials. *Progress of Theoretical Physics Supplement*, 159, 326–337.
- Aksu, E. (2013). Study of MgB₂ phase formation by using XRD, SEM, thermal and magnetic measurements. *Journal of Alloys and Compounds*, 552, 376–381.
- Aldica, G., Popa, S., Enculescu, M., Pasuk, I., Ionescu, A.M., and Badica, P. (2018). Dwell time influence on spark plasma-sintered MgB₂. *Journal of Superconductivity and Novel Magnetism*, 31, 317–325.
- Aruldas, G., and P. Rajagopal. (2006). *Modern physics* (Second Edi). New Delhi: Prentice-Hall of India Pvt. Ltd.
- Arvapalli, S.S., Miryala, M., and Murakami, M. (2019). Beneficial impact of excess Mg on flux pinning in bulk MgB₂ synthesized with Ag addition and carbon encapsulated boron. *Advanced Engineering Materials*, 21, 1900497.
- Arvapalli, S.S., Muralidhar, M., and Murakami, M. (2019). High-performance bulk MgB₂ superconductor using amorphous nano-boron. *Journal of Superconductivity and Novel Magnetism*, 32, 1891–1895.
- Balducci, G., Brutti, S., Ciccio, A., Gigli, G., Manfrinetti, P., Palenzona, A., Butman, M.F., and Kudin, L. (2005). Thermodynamics of the intermediate phases in the Mg-B system. *Journal of Physics and Chemistry of Solids*, 66, 292–297.
- Bardeen, J., Cooper, L.N., and Schrieffer, J.R. (1957). Microscopic theory of superconductivity. *Physical Review*, 108, 162–164.
- Bednorz, J.G., and Muller, K.A. (1986). Possible high T_c superconductivity in the Ba-La-Cu-O system. *Condensed Matter*, 64, 189–193.
- Braccini, V., Malagoli, A., Tumino, A., Vignolo, M., Bernini, C., Fanciulli, C., Romano, G., Tropeano, M., Siri, A.S., and Grasso, G. (2007). Improvement of magnetic field behavior of *ex-situ* processed magnesium diboride tapes. *IEEE Transactions on Applied Superconductivity*, 17, 2766–2769.
- Brutti, S., Ciccio, A., Balducci, G., Gigli, G., Manfrinetti, P., and Palenzona, A. (2002). Vaporization thermodynamics of MgB₂ and MgB₄. *Applied Physics Letters*, 80, 2892–2894.
- Bruzek, C.E., Ballarino, A., Escamez, G., Giannelli, S., Grilli, F., Lesur, F., Marian, A., & Tropeano, M. (2017). Cable conductor design for the high-power MgB₂ DC superconducting cable project of BEST PATHS. *IEEE Transactions on Applied Superconductivity*, 27, 4801405.
- Bruzek, C.E., and Marian, A. (2021). Superconducting links for very high power transmission based on MgB₂ wires. *Conference: 2021 AEIT HVDC International*

Conference (AEIT HVDC).

- Buzea, C., and Yamashita, T. (2001). Review of the superconducting properties of MgB₂. *Superconductor Science and Technology*, 14, R115–R146.
- Canfield, P.C., and Crabtree, G.W. (2003). Magnesium diboride: Better late than never. *Physics Today*, 56, 34–40.
- Chen, D.X., and Goldfarb, R.B. (1989). Kim model for magnetization of type-II superconductors. *Journal of Applied Physics*, 66, 2489–2500.
- Chen, H., Li, Y., Chen, G., Xu, L., and Zhao, X. (2018). The effect of inhomogeneous phase on the critical temperature of smart meta-superconductor MgB₂. *Journal of Superconductivity and Novel Magnetism*, 31, 3175–3182.
- Chen, L., and Li, H. (2003). Superconducting properties of MgB₂ with different lattice parameters. *Chinese Physics Letters*, 20, 1128–1130.
- Chen, S.K., Serquis, A., Serrano, G., Yates, K.A., Blamire, M.G., Guthrie, D., Cooper, J., Wang, H., Margadonna, S., and MacManus-Driscoll, J.L. (2008). Structural and superconducting property variations with nominal Mg non-stoichiometry in Mg_xB₂ and its enhancement of upper critical field. *Advanced Functional Materials*, 18, 113–120.
- Chen, S.K., Wei, M., and MacManus-Driscoll, J.L. (2006). Strong pinning enhancement in MgB₂ using very small Dy₂O₃ additions. *Applied Physics Letters*, 88, 192512.
- Choi, H.J., Roundy, D., Sun, H., Cohen, M.L., and Louie, S.G. (2002). The origin of the anomalous superconducting properties of MgB₂. *Nature*, 418, 758–760.
- Collings, E.W., Sumption, M.D., Bhatia, M., Susner, M.A., and Bohnenstiehl, S.D. (2008). Prospects for improving the intrinsic and extrinsic properties of magnesium diboride superconducting strands. *Superconductor Science and Technology*, 21, 103001.
- Cooley, L.D., Kang, K., Klie, R.F., Li, Q., Moodenbaugh, A.M., and Sabatini, R.L. (2004). Formation of MgB₂ at low temperatures by reaction of Mg with B₆Si. *Superconductor Science and Technology*, 17, 942–946.
- Cyrot, M. (1973). Ginzburg-Landau theory for superconductors. *Reports on Progress in Physics*, 36, 103–158.
- Cyrot, M., and Pavuna, D. (1992). *Introduction to superconductivity and high-T_c materials*. World Scientific Publishing Co. Pte. Ltd.
- Dahm, T. (2005). Two-gap superconductivity in magnesium diboride. *Advances in Solid State Physics*, 45, 239–249.
- De la Mora, P., Castro, M., and Tavizon, G. (2002). Comparative study of the electronic structure of alkaline-earth borides (MeB₂; Me = Mg, Al, Zr, Nb, and Ta) and their normal-state conductivity. *Journal of Solid State Chemistry*, 169, 168–175.

- Degen, T., Sadki, M., Bron, E., König, U., and Nénert, G. (2014). The high score suite. *Powder Diffraction*, 29, S13–S18.
- Dew-Hughes, D. (1974). Flux pinning mechanisms in type II superconductors. *Philosophical Magazine*, 30, 293–305.
- Dou, S.X., Pan, A.V., Zhou, S., Ionescu, M., Liu, H.K., and Munroe, P.R. (2002). Substitution-induced pinning in MgB₂ superconductor doped with SiC nanoparticles. *Superconductor Science and Technology*, 15, 1587–1591.
- Durrant, A. (2000). *Quantum Physics of Matter*. United States: CRC Press.
- Eisterer, M. (2008). Calculation of the volume pinning force in MgB₂ superconductors. *Physical Review B*, 77, 144524.
- Eom, C.B., Lee, M.K., Choi, J.H., Belenky, L.J., Song, X., Cooley, L.D., Naus, M.T., Patnaik, S., Jiang, J., Rikel, M., Polyanskii, A., Gurevich, A., Cai, X.Y., Bu, S.D., Babcock, S.E., Hellstrom, E.E., Larbalestier, D. C., Rogado, N., Regan, K.A., Hayward, M.A., He, T., Slusky, J.S., Inumaru, K., Haas, M.K., and Cava, R.J. (2001). High critical current density and enhanced irreversibility field in superconducting MgB₂ thin films. *Nature*, 411, 558–560.
- Fan, Z.Y., Hinks, D.G., Newman, N., and Rowell, J.M. (2001). Experimental study of MgB₂ decomposition. *Applied Physics Letters*, 79, 87–89.
- Fang, C., Huang, B., Yang, X., He, K., Chen, L., Shi, A., Zhang, Z., and Huang, Q. (2020). Effects of LaB₆ on the microstructures and ablation properties of 3D C/C-SiC-ZrB₂-LaB₆ composites. *Journal of the European Ceramic Society*, 40, 2781–2790.
- Forrest, A.M. (1983). Meissner and ochenfeld revisited. *European Journal of Physics*, 4, 117–120.
- Fuchs, G., Müller, K.H., Handstein, A., Nenkov, K., Narozhnyi, V.N., Eckert, D., Wolf, M., and Schultz, L. (2001). Upper critical field and irreversibility line in superconducting MgB₂. *Solid State Communications*, 118, 497–501.
- Gao, Z., Ma, Y., Wang, D., and Zhang, X. (2010). Development of doped MgB₂ wires and tapes for practical applications. *IEEE Transactions on Applied Superconductivity*, 20, 1515–1520.
- Gao, Z.S., Ma, Y.W., Wang, D.L., Zhang, X.P., Awaji, S., and Watanabe, K. (2010). Enhancement of critical current density and flux pinning in acetone and La₂O₃ codoped MgB₂ tapes. *Chinese Physics Letters*, 27, 117401.
- Ginzburg, V. L., and E. A. Andryushin. (2004). *Superconductivity* (Revised Edition). Singapore: World Scientific Publishing Co. Pte. Ltd.
- Giunchi, G., Ripamonti, G., Raineri, S., Botta, D., Gerbaldo, R., and Quarantiello, R. (2004). Grain size effects on the superconducting properties of high density bulk MgB₂. *Superconductor Science and Technology*, 17, S583–S588.

- Glowacki, B.A., Kutukcu, M.N., Atamert, S., Dhulst, C., and Mestdagh, J. (2019). Formation of Mg₂Si inclusions in *in situ* SiC doped MgB₂ wires made from variable concentration of large micrometer-size Mg powder by continuous method. *IOP Conference Series: Materials Science and Engineering*, 502, 2–7.
- Guo, Y., Zhang, W., Yang, D., and Yao, R.L. (2012). Decomposition and oxidation of magnesium diboride. *Journal of the American Ceramic Society*, 95, 754–759.
- Gupta, A., Kumar, A., and Narlikar, A.V. (2009). Normal state connectivity and J_c of weakly coupled MgB₂ particles. *Superconductor Science and Technology*, 22, 105005.
- Hapipi, N.M., Miryala, M., Chen, S.K., Arvapalli, S.S., Murakami, M., Kechik, M.M.A., Tan, K.B., and Lee, O.J. (2020). Enhancement of critical current density for MgB₂ prepared using carbon-encapsulated boron with co-addition of Dy₂O₃ and La₂O₃. *Ceramics International*, 46, 23041–23048.
- Häßler, W., Scheiter, J., Hädrich, P., Kauffmann-Weiß, S., Holzapfel, B., Oomen, M., and Nielsch, K. (2018). Properties of *ex-situ* MgB₂ bulk samples prepared by uniaxial hot pressing and spark plasma sintering. *Physica C*, 551, 48–54.
- Hayashi, K. (2020). Commercialization of Bi-2223 superconducting wires and their applications. *SEI Technical Review*, 91, 68–74.
- Higuchi, M., Muralidhar, M., Jirsa, M., and Murakami, M. (2017). Microstructure and critical current density in MgB₂ bulk made of 4.5 wt% carbon-coated boron. *Journal of Physics: Conference Series*, 871, 012059.
- Hinks, D.G., Jorgensen, J.D., Zheng, H., and Short, S. (2002). Synthesis and stoichiometry of MgB₂. *Physica C*, 382, 166–176.
- Jones, M.E., and Marsh, R.E. (1953). Formation of MgB₂ phase with interaction of Mg and amorphous B. *Journal of the American Chemical Society*, 76, 870.
- Jung, S.G., Seong, W.K., and Kang, W.N. (2012). Effect of columnar grain boundaries on flux pinning in MgB₂ films. *Journal of Applied Physics*, 111, 053906.
- Kario, A., Nast, R., Häler, W., Rodig, C., Mickel, C., Goldacker, W., Holzapfel, B., and Schultz, L. (2011). Critical current density enhancement in strongly reactive *ex-situ* MgB₂ bulk and tapes prepared by high energy milling. *Superconductor Science and Technology*, 24, 075011.
- Khachan, J., and Bosi, S. (2003). *Superconductivity*. Brookhaven National Laboratory, University of California, Santa Barbara.
- Kim, J.H., Dou, S.X., Shi, D.Q., Rindfleisch, M., and Tomsic, M. (2007). Study of MgO formation and structural defects in *in situ* processed MgB₂/Fe wires. *Superconductor Science and Technology*, 1026, 1–7.
- Kim, J.H., Dou, S.X., Wang, J.L., Shi, D.Q., Xu, X., Hossain, M.S.A., Yeoh, W.K., Choi, S., and Kiyoshi, T. (2007). The effects of sintering temperature on

superconductivity in MgB₂/Fe wires. *Superconductor Science and Technology*, 20, 448–451.

Kim, Jung Ho, Oh, S., Heo, Y.U., Hata, S., Kumakura, H., Matsumoto, A., Mitsuhashi, M., Choi, S., Shimada, Y., Maeda, M., MacManus-Driscoll, J.L., and Dou, S.X. (2012). Microscopic role of carbon on MgB₂ wire for critical current density comparable to NbTi. *NPG Asia Materials*, 4, e3-7.

Kimishima, Y., Uehara, M., Kuramoto, T., Takano, S., and Takami, S. (2004). La-doping effects on pinning properties of MgB₂. *Physica C*, 412–414, 402–406.

Kobayashi, H., Muralidhar, M., Koblishka, M.R., Inoue, K., and Murakami, M. (2015). Improvement in the performance of bulk MgB₂ material through optimization of sintering process. *Physics Procedia*, 65, 73–76.

Kortus, J., Mazin, I.I., Belashchenko, K.D., Antropov, V.P., and Boyer, L.L. (2001). Superconductivity of metallic boron in MgB₂. *Physical Review Letters*, 86, 4656–4659.

Kortus, J., Dolgov, O.V., Kremer, R.K., and Golubov, A.A. (2005). Band filling and interband scattering effects in MgB₂: Carbon versus aluminum doping. *Physical Review Letters*, 94, 027002.

Kováč, P., Hušek, I., Melišek, T., Rosová, A., and Dobročka, E. (2021). Effect of grain size selection in *ex-situ* made MgB₂ wires. *Physica C*, 583, 1353826.

Kováč, P., Hušek, I., Rosová, A., Kulich, M., Kováč, J., Melišek, T., Kopera, L., Balog, M., and Krížik, P. (2018). Ultra-lightweight superconducting wire based on Mg, B, Ti and Al. *Scientific Reports*, 8, 11229.

Kováč, P., Reissner, M., Melišek, T., Hušek, I., and Mohammad, S. (2009). Current densities of MgB₂ wires by combined *ex situ/in situ* process. *Journal of Applied Physics*, 106, 013910.

Langford, J.I., and Wilson, A.J.C. (1978). Scherrer after sixty years: A survey and some new results in the determination of crystallite size. *Journal of Applied Crystallography*, 11, 102–113.

Larbalestier, D.C., Cooley, L.D., Rikel, M.O., Polyanskii, A.A., Jiang, J., Patnaik, S., Cai, X. Y., Feldmann, D.M., Gurevich, A., Squitieri, A.A., Naus, M.T., Eom, C. B., Hellstrom, E. E., Cava, R.J., Regan, K.A., Rogado, N., Hayward, M.A., He, T., Slusky, J.S., Khalifah, P., Inumaru, K., and Haas, M. (2001). Strongly linked current flow in polycrystalline forms of the superconductor MgB₂. *Nature*, 410, 186–189.

Li, W.X., Zeng, R., Wang, J.L., Li, Y., and Dou, S.X. (2012). Dependence of magnetoelectric properties on sintering temperature for nano-SiC-doped MgB₂/Fe wires made by combined *in situ/ex situ* process. *Journal of Applied Physics*, 111, 07E135.

Liao, X.Z., Serquis, A., Zhu, Y.T., Huang, J.Y., Civale, L., Peterson, D.E., Mueller, F.M.,

- and Xu, H.F. (2003). Mg(B,O)₂ precipitation in MgB₂. *Journal of Applied Physics*, 93, 6208–6215.
- Liu, A.Y., Mazin, I.I., and Kortus, J. (2001). Beyond eliasberg superconductivity in MgB₂: Anharmonicity, two-phonon scattering, and multiple gaps. *Physical Review Letters*, 87, 87005.
- Liu, C.F., Yan, G., Du, S.J., Xi, W., Feng, Y., Zhang, P.X., Wu, X.Z., and Zhou, L. (2003). Effect of heat-treatment temperatures on density and porosity in MgB₂ superconductor. *Physica C*, 386, 603–606.
- Liu, H.K., Zhou, S.H., Soltanian, S., Horvat, J., Pan, A.V., Qin, M.J., Wang, X.L., Lonescu, M., and Dou, S. X. (2003). Effect of nano-SiC and nano-Si doping on critical current density of MgB₂. *Tsinghua Science and Technology*, 8, 307–315.
- Liu, H., Li, J., Sun, M., Qu, J., Zheng, R., Cairney, J. M., Zhu, M., Li, Y., and Li, W. (2020). Carbon-coating layers on boron generated high critical current density in MgB₂ superconductor. *ACS Applied Materials and Interfaces*, 12, 8563–8572.
- Liu, Y., Qin, J., Ke, C., Cheng, C., Zhou, D., Zhang, Y., and Zhao, Y. (2022). Enhanced flux pinning by magnetic CrB₂ nanoparticle in MgB₂ superconductor. *Journal of Magnetism and Magnetic Materials*, 551, 169174.
- London, F., and London, H. (1935). The electromagnetic equations of the supraconductor. In *Proceedings of the Royal Society of London. Series A, Mathematical and Physical Sciences*, 149, 71–88.
- Maeda, H., Tanaka, Y., Fukutomi, M., and Asano, T. (1988). A new high-*T_c* oxide superconductor without a rare earth element. *Japanese Journal of Applied Physics*, 27, L209–L210.
- Malagoli, A., Braccini, V., Bernini, C., Romano, G., Vignolo, M., Putti, M., and Ferdeghini, C. (2010). Study of the MgB₂ grain size role in *ex-situ* multifilamentary wires with thin filaments. *Superconductor Science and Technology*, 23, 025032.
- Matsushita, T. (2014). *Flux Pinning in Superconductors*; 2nd ed.; New York: Springer Series in Solid-State Sciences.
- Matthews, G.A.B., Liu, J., Grovenor, C.R.M., Grant, P.S., and Speller, S. (2020). Design and characterisation of *ex-situ* bulk MgB₂ superconductors containing a nanoscale dispersion of artificial pinning centres. *Superconductor Science and Technology*, 33, 034006.
- Matthews, G.A.B., Santra, S., Ma, R., Grovenor, C.R.M., Grant, P.S., and Speller, S.C. (2020). Effect of the sintering temperature on the microstructure and superconducting properties of MgB₂ bulks manufactured by the field assisted sintering technique. *Superconductor Science and Technology*, 33, 054003.
- Mizutani, S., Yamamoto, A., Shimoyama, J.I., Ogino, H., and Kishio, K. (2014). Self-sintering-assisted high intergranular connectivity in ball-milled *ex-situ* MgB₂

- bulks. *Superconductor Science and Technology*, 27, 114001.
- Moshchalkov, V., Menghini, M., Nishio, T., Chen, Q.H., Silhanek, A.V, Dao, V.H., Chibotaru, L.F., Zhigadlo, N.D., and Karpinski, J. (2009). Type-1.5 superconductivity. *Physical Review Letters*, 102, 117001.
- Mourachkine, A. (2002). *High-temperature superconductivity in cuprates*. Kluwer Academic Publishers.
- Muralidhar, M., Higuchi, M., Diko, P., Jirsa, M., and Murakami, M. (2017). Record critical current density in bulk MgB₂ using carbon-coated amorphous boron with optimum sintering conditions. *Journal of Physics: Conference Series*, 871, 012056.
- Muralidhar, M., Higuchi, M., Jirsa, M., Diko, P., Kokal, I., and Murakami, M. (2017). Improved critical current densities of bulk MgB₂ using carbon-coated amorphous boron. *IEEE Transactions on Applied Superconductivity*, 27, 6201104.
- Muralidhar, M., Higuchi, M., Kitamoto, K., Koblichka, M.R., Jirsa, M., and Murakami, M. (2018). Enhanced critical current density in bulk MgB₂. *IEEE Transactions on Applied Superconductivity*, 28, 8000405.
- Muralidhar, M., Kenta, N., Koblichka, M.R., and Murakami, M. (2015). High critical current densities in bulk MgB₂ fabricated using amorphous boron. *Physica Status Solidi (A) Applications and Materials Science*, 212, 2141–2145.
- Muralidhar, M., Kitamoto, K., Arvapalli, S.S., Das, D., Jirsa, M., Murakami, M., Ramachandra, S., and Mamidanna, R. (2022). Enhancing critical current density of bulk MgB₂ via nanoscale boron and Dy₂O₃ doping. *Advanced Engineering Materials*, 24, 2200487.
- Muralidhar, M., Nozaki, K., Kobayashi, H., Zeng, X.L., Koblichka-Veneva, A., Koblichka, M.R., Inoue, K., and Murakami, M. (2015). Optimization of sintering conditions in bulk MgB₂ material for improvement of critical current density. *Journal of Alloys and Compounds*, 649, 833–842.
- Nagamatsu, J., Nakagawa, N., Muranaka, T., Zenitani, Y., and Akimitsu, J. (2001). Superconductivity at 39 K in magnesium diboride. *Nature*, 410, 2–3.
- Nagarajan, R., Mazumdar, C., Hossain, Z., Dhar, S.K., Gopalakrishnan, K.V., Gupta, L.C., Godart, C., Padalia, B.D., and Vijayaraghavan, R. (1994). Bulk superconductivity at an elevated temperature (T = 12 K) in a nickel containing alloy system Y-Ni-B-C. *Physical Review Letters*, 72, 274–277.
- Nakane, T., Jiang, C.H., Mochiku, T., Fujii, H., Kuroda, T., and Kumakura, H. (2005). Effect of SiC nanoparticle addition on the critical current density of MgB₂ tapes fabricated from MgH₂, B and MgB₂. *Superconductor Science and Technology*, 18, 1337–1341.
- Narlikar, A. V. (1995). *Field Penetration and Magnetization of High Temperature Superconductors*. New York: Nova Science Publisher, Inc.

- Nishibori, E., Takata, M., Sakata, M., Tanaka, H., Muranaka, T., and Akimitsu, J. (2001). Bonding nature in MgB₂. *Journal of the Physical Society of Japan*, 70, 2252–2254.
- Ohmichi, E., Masui, T., Lee, S., Tajima, S., and Osada, T. (2004). Enhancement of irreversibility field in carbon-substituted MgB₂ single crystals. *Journal of Physical Society of Japan*, 73, 2065–2068.
- Onar, K., Balci, Y., and Yakinci, M.E. (2014). Effect of grain size on the electrical and magnetic properties of MgB₂ thick films deposited on the Al₂O₃ single crystal substrates. *Journal of Materials Science: Materials in Electronics*, 25, 2104–2110.
- Pan, A.V., Zhou, S., Liu, H., and Dou, S. (2003). Properties of superconducting MgB₂ wires: *In situ* versus *ex situ* reaction technique. *Superconductor Science and Technology*, 16, 639–644.
- Peng, J., Cai, Q., Cheng, F., Ma, Z., Li, C., Xin, Y., and Liu, Y. (2017). Enhancement of critical current density by a “MgB₂-MgB₄” reversible reaction in self-sintered *ex situ* MgB₂ bulks. *Journal of Alloys and Compounds*, 694, 24–29.
- Poole, C. P., Farach, H. A., Creswick, R. J., and Prozorov, R. (2014). *Superconductivity* (Third edition). Amsterdam: Elsevier.
- Putilin, S.N., Antipov, E.V., Chmaissem, O., and Marezio, M. (1993). Superconductivity at 94 K in HgBa₂CuO_{4+d}. *Letters to Nature*, 362, 226–228.
- Rafieazad, M., Balci, Ö., Acar, S., and Somer, M. (2017). Review on magnesium diboride (MgB₂) as excellent superconductor: Effects of the production techniques on the superconducting properties. *Journal of Boron*, 2, 87–96.
- Rahul, R., Thomas, S., K.M., D., Varghese, N., Paulose, A.P., Varma, M.R., and Syamaprasad, S. (2017). Tackling the agglomeration of Mg₂Si dopant in MgB₂ superconductor using cast Mg–Si alloy. *Materials Research Bulletin*, 93, 296–302.
- Ray, P. J. (2015). *Structural investigation of La_{2-x}Sr_xCuO_{4+y} - Following staging as a function of temperature* (Issue November). University of Copenhagen, Denmark.
- Rose-Innes, A. C., and E.H. Rhoderick. (1978). *Introduction to superconductivity* (Second Edition). New York: Pergamon Press.
- Russell, V., Hirst, R., Kanda, F.A., and King, A.J. (1953). An X-ray study of the magnesium borides. *Acta Crystallographica*, 6, 870.
- Schmidt, V. V., Muller, P., and Ustinov, A. V. (1997). *The Physics of Superconductors: Introduction to Fundamentals and Applications*. New York: Springer Science & Business Media.
- Schmitt, R., Glaser, J., Wenzel, T., Nickel, K.G., and Meyer, H.J. (2006). A reactivity study in the Mg–B system reaching for an improved synthesis of pure MgB₂. *Physica C*, 436, 38–42.
- Shahabuddin, M., Alzayed, N.S., Oh, S., Choi, S., Maeda, M., Hata, S., Shimada, Y.,

- Hossain, M.S. Al, and Kim, J.H. (2014). Microstructural and crystallographic imperfections of MgB₂ superconducting wire and their correlation with the critical current density. *AIP Advances*, 4, 017113.
- Shekhar, C., Giri, R., Tiwari, R.S., and Srivastava, O.N. (2004). On the synthesis and characterization of La doped MgB₂ superconductor. *Crystal Research and Technology*, 29, 718–725.
- Shekhar, C., Giri, R., Tiwari, R.S., Rana, D.S., Malik, S.K., and Srivastava, O.N. (2005). Effect of La doping on microstructure and critical current density of MgB₂. *Superconductor Science and Technology*, 18, 1210–1214.
- Sheng, Z.Z., and Hermann, A.M. (1988). Bulk superconductivity at 120 K in the Tl-Ca/Ba-Cu-O system. *Nature*, 332, 138–139.
- Shim, S.H., Shim, K.B., and Yoon, J. (2005). Superconducting characteristics of polycrystalline magnesium diboride ceramics fabricated by a spark plasma sintering technique. *Journal of the American Ceramic Society*, 88, 858–861.
- Shimada, Y., Hata, S., Ikeda, K.I., Nakashima, H., Matsumura, S., Tanaka, H., Yamamoto, A., Shimoyama, J.I., and Kishio, K. (2015). Microstructural characteristics of ball-milled self-sintered *ex-situ* MgB₂ bulks. *IEEE Transactions on Applied Superconductivity*, 25, 6801105.
- Shimada, Y., Hata, S., Ikeda, K.I., Nakashima, H., Matsumura, S., Tanaka, H., Yamamoto, A., Shimoyama, J.I., and Kishio, K. (2016). Microstructural connectivity in sintered *ex-situ* MgB₂ bulk superconductors. *Journal of Alloys and Compounds*, 656, 172–180.
- Sinha, B.B., Kadam, M.B., Mudgel, M., Awana, V.P.S., Kishan, H., and Pawar, S.H. (2010). Synthesis and characterization of excess magnesium MgB₂ superconductor under inert carbon environment. *Physica C*, 470, 25–30.
- Soltanian, S., Wang, X., Horvat, J., Qin, M., Liu, H., Munroe, P.R., and Dou, S.X. (2003). Effect of grain size and doping level of SiC on the superconductivity and critical current density in MgB₂ superconductor. *IEEE Transactions on Applied Superconductivity*, 13, 3273–3276.
- Suhl, H., Matthias, B.T., and Walker, L.R. (1959). Bardeen-Cooper-Schrieffer theory in the case of overlapping bands. *Physical Review Letters*, 3, 552–554.
- Superconducting feeder cable system*. Railway Technical Research Institute. (n.d.). Retrieved August 6, 2019, from https://www.rtri.or.jp/eng/press/2019/nr201904_detail.html
- Suryanarayana, C., and Norton, M. G. (2013). *X-ray diffraction: A practical approach*. New York: Springer Science & Business Media.
- Tan, K.L., Tan, K.Y., Lim, K.P., Shaari, A.H., and Chen, S.K. (2012). Optimization of phase formation and superconducting properties in MgB₂ prepared by phase transformation from MgB₄. *Journal of Electronic Materials*, 41, 673–678.

- Tan, K.Y., Tan, K.L., T., Tan, K.B., Lim, K.P., Halim, S.A., and Chen, S.K. (2011). Enhanced critical current density in MgB₂ superconductor via Si and C coadditions. *Journal of Superconductivity and Novel Magnetism*, 24, 2025–2029.
- Tan, K.Y., Tan, K.B., Lim, K.P., Halim, S.A., and Chen, S.K. (2015). Effect of sintering temperature on the superconducting properties of MgB₂ superconductor co-added with a high concentration of Si and C. *Advanced Materials Research*, 1107, 589–594.
- Tanaka, H., Yamamoto, A., Shimoyama, J.I., Ogino, H., and Kishio, K. (2012). Strongly connected *ex-situ* MgB₂ polycrystalline bulks fabricated by solid-state self-sintering. *Superconductor Science and Technology*, 25, 115022.
- Tzeli, D., and Mavridis, A. (2005). Ab initio investigation of the electronic and geometric structure of magnesium diboride, MgB₂. *Journal of Physical Chemistry A*, 109, 10663–10674.
- Verma, N. K. (2017). *Physics for Engineers* (Second Edi). New Delhi: PHI Learning Pvt. Ltd.
- Vinod, K., Varghese, N., Roy, S.B., and Syamaprasad, U. (2009). Significant enhancement of the in-field critical current density of the MgB₂ superconductor through codoping of nano-TiC with nano-SiC. *Superconductor Science and Technology*, 22, 055009.
- Wan, F., Sumption, M.D., and Collings, E.W. (2023). Mechanism of enhanced critical fields and critical current densities of MgB₂ wires with C/Dy₂O₃ co-additions. *Journal of Applied Physics*, 133, 023905.
- Wang, J., Bugoslavsky, Y., Berenov, A., Cowey, L., Caplin, A.D., Cohen, L.F., MacManus Driscoll, J.L., Cooley, L.D., Song, X., and Larbalestier, D.C. (2002). High critical current density and improved irreversibility field in bulk MgB₂ made by a scaleable, nanoparticle addition route. *Applied Physics Letters*, 81, 2026–2028.
- Wang, X.L., Zhou, S.H., Qin, M.J., Munroe, P.R., Soltanian, S., Liu, H.K., and Dou, S.X. (2003). Significant enhancement of flux pinning in MgB₂ superconductor through nano-Si addition. *Physica C*, 385, 461–465.
- Warren, N. (2003). *Excel HSC Physics (New Edition)*. New South Wales: Pascal Press.
- Wu, F. (2014). The improved superconducting properties in the *ex-situ* sintered MgB₂ bulks with Mg addition. *Journal of Low Temperature Physics*, 177, 157–164.
- Wu, M.K., Ashburn, J.R., Torng, C.J., Hor, P.H., Meng, R.L., Gao, L., Huang, Z.J., Wang, Y. Q., and Chu, C.W. (1987). Superconductivity at 93 K in a new mixed-phase Y-Ba-Cu-O compound system at ambient pressure. *Physical Review Letters*, 58, 908–910.
- Xu, M., Kitazawa, H., Takano, Y., Ye, J., Nishida, K., Abe, H., Matsushita, A., and Kido, G. (2001). Single crystal MgB₂ with anisotropic superconducting properties.

Applied Physics Letters, 79, 1–7.

- Yamamoto, A., Shimoyama, J.I., Kishio, K., and Matsushita, T. (2007). Limiting factors of normal-state conductivity in superconducting MgB₂: An application of mean-field theory for a site percolation problem. *Superconductor Science and Technology*, 20, 658–666.
- Yamamoto, A., Shimoyama, J.I., Ueda, S., Katsura, Y., Horii, S., and Kishio, K. (2004). Synthesis of high J_c MgB₂ bulks with high reproducibility by a modified powder-in-tube method. *Superconductor Science and Technology*, 17, 921–925.
- Yamamoto, A., Tanaka, H., Shimoyama, J.I., Ogino, H., Kishio, K., and Matsushita, T. (2012). Towards the realization of higher connectivity in MgB₂ conductors: *In-situ* or sintered *ex-situ*? *Japanese Journal of Applied Physics*, 51, 010105.
- Yan, G., Feng, Y., Fu, B.Q., Liu, C.F., Zhang, P.X., Wu, X.Z., Zhou, L., Zhao, Y., and Pradhan, A.K. (2004). Effect of synthesis temperature on density and microstructure of MgB₂ superconductor at ambient pressure. *Journal of Materials Science*, 39, 4893–4898.
- Yang, D., Sun, H., Lu, H., Guo, Y., Li, X., and Hu, X. (2003). Experimental study on the oxidation of MgB₂ in air at high temperature. *Superconductor Science and Technology*, 16, 576–581.
- Yang, Y., Sumption, M.D., and Collings, E.W. (2016). Influence of metal diboride and Dy₂O₃ additions on microstructure and properties of MgB₂ fabricated at high temperatures and under pressure. *Scientific Reports*, 6, 29306.
- Yeoh, W.K., Horvat, J., Dou, S.X., and Keast, V. (2004). Strong pinning and high critical current density in carbon nanotube doped MgB₂. *Superconductor Science and Technology*, 17, S572–S577.
- Yildirim, T. (2002). The surprising superconductor. *Materials Today*, 40–44.
- Zeng, R., Lu, L., Li, W. X., Wang, J.L., Shi, D.Q., Horvat, J., Dou, S.X., Bhatia, M., Sumption, M., Collings, E.W., Yoo, J.M., Tomsic, M., and Rindfleisch, M. (2008). Excess Mg addition MgB₂/Fe wires with enhanced critical current density. *Journal of Applied Physics*, 103, 083911.
- Zeng, R., Lu, L., Wang, J.L., Horvat, J., Li, W.X., Shi, D.Q., Dou, S.X., Tomsic, M., and Rindfleisch, M. (2007). Significant improvement in the critical current density of *in situ* MgB₂ by excess Mg addition. *Superconductor Science and Technology*, 20, L43–L47.
- Zhang, C.Y., Wang, Y.B., Hu, W.W., and Feng, Q.R. (2010). The effect of Si addition in MgB₂ thin films by hybrid physical-chemical vapor deposition using silane as the doping source. *Superconductor Science and Technology*, 23, 065017.
- Zhang, H., Li, L., Zhao, Y., and Zhang, Y. (2017). The performance improvement of MgB₂ prepared by the Mg diffusion method with the MgB₄ addition. *Journal of Physics: Conference Series*, 871, 012057.

- Zhang, H., Zhao, Y., and Zhang, Y. (2015). The effects of excess Mg addition on the superconductivity of MgB₂. *Journal of Superconductivity and Novel Magnetism*, 28, 8–11.
- Zhang, Y., Lu, C., Zhou, S.H., Chung, K.C., Kim, Y.K., and Dou, S.X. (2009). Influence of heat treatment on superconductivity of MgB₂ bulk sintered in flowing welding grade Ar atmosphere. *IEEE Transactions on Magnetics*, 45, 2626–2629.
- Zhang, Y., Lu, C., Zhou, S.H., Chung, K.C., Kim, Y.K., and Dou, S.X. (2009). Influence of heat treatment on the critical current density of MgB₂ bulk sintered in vacuum and flowing welding grade Ar atmosphere. *IEEE Transactions on Magnetics*, 45, 2626–2629.
- Zhang, Y., Zhou, S.H., Lu, C., Chung, K.C., and Dou, S.X. (2009). Effect of sintering time on superconductivity in MgB₂. *International Journal of Modern Physics B*, 23, 3476–3481.
- Zhao, Y., Feng, Y., Cheng, C.H., Zhou, L., Wu, Y., Machi, T., Fudamoto, Y., Koshizuka, N., and Murakami, M. (2001). High critical current density of MgB₂ bulk superconductor doped with Ti and sintered at ambient pressure. *Applied Physics Letters*, 79, 1154–1156.
- Zhao-Shun, G.O, Yan-Wei, M., Dong-Liang, W., Xian-Ping, Z., Satoshi, A., and Kazuo, W. (2010). Enhancement of critical current density and flux pinning in acetone and La₂O₃ codoped MgB₂ tapes. *Chinese Physics Letters*, 27, 11740.